Practical Considerations for Optimal Mismatched Filtering of Nonrepeating Waveforms

Matthew B. Heintzelman[1], Jonathan W. Owen[1], Shannon D. Blunt[1], Brianna Maio[2], Eric D. Steinbach[2]
[1]Radar Systems Lab (RSL), University of Kansas, Lawrence KS
[2]Sandia National Laboratories, Albuquerque, NM

***Abstract* – We consider the intersection between nonrepeating random FM (RFM) waveforms and practical forms of optimal mismatched filtering (MMF). Specifically, the spectrally-shaped inverse filter (SIF) is a well-known approximation to the least-squares (LS-MMF) that provides significant computational savings. Given that nonrepeating waveforms likewise require unique nonrepeating MMFs, this efficient form is an attractive option. Moreover, both RFM waveforms and the SIF rely on spectrum shaping, which establishes a relationship between the goodness of a particular waveform and the mismatch loss (MML) the corresponding filter can achieve. Both simulated and open-air experimental results are shown to demonstrate performance.**

Keywords–mismatched filtering, inverse filtering, least squares, waveform diversity, noise waveforms

I. Introduction

Nonrepeating random FM (RFM) waveforms, shaped to provide good spectral containment, have been experimentally demonstrated for a variety of applications and design approaches (see [1] and references therein). Because they possess a thumbtack ambiguity function, individual RFM waveforms cannot attain quite the degree of low sidelobe performance, as a function of time-bandwidth product (TB), that is achievable with optimized chirp-like structures [2,3]. While slow-time combining (e.g. Doppler/cross-range processing) of M unique RFM waveforms does realize a $\sim 10\log_{10}(M)$ incoherent averaging suppression of sidelobes [1], the use of appropriate mismatched filtering (e.g. [4-15]) provides even further suppression for when high dynamic range is required.

Due to the Fourier relationship between spectral density and autocorrelation, RFM waveform design in terms of the former naturally addresses the latter. Here we examine how the spectral density perspective for optimized MMF design is impacted by this manner of waveform design. Specifically, the spectrally-shaped inverse filter (SIF) is assessed relative to iterative waveform optimization that is driven to conform to a given spectral template. It is consequently shown that this shared (yet not actually joint) optimization formulation, in which both waveform and filter design are based on the same/similar spectral template(s), provides meaningful sidelobe suppression performance in a computationally efficient manner when the underlying model assumptions are valid. The impact of violating the model assumption is likewise examined. Further, while we specifically examine LS-MMF and SIF in the context of RFM waveforms, the filter considerations are applicable to arbitrary waveform structures as well.

II. The Convolution Model

The well-known LS-MMF formulation [4] provides a closed-form solution to determine an optimal filter based on the discretized convolution model. This model can be expressed in the matrix form $\mathbf{y} = \mathbf{S}\mathbf{x} + \mathbf{v}$, with L-length vector $\mathbf{x}$ comprising the true scattering, $\mathbf{v}$ a vector of additive noise, and $\mathbf{y}$ the length $L+N-1$ resulting received signal. The $(L+N-1)\times L$ Toeplitz matrix $\mathbf{S}$ then contains a delay-shifted (and otherwise zero-padded) N-length discretized version $\mathbf{s}$ of waveform $s(t)$ in the columns. Matched filtering can then be represented as

$$\hat{\mathbf{x}} = \mathbf{S}^H\mathbf{y} = \mathbf{S}^H\mathbf{S}\mathbf{x} + \mathbf{S}^H\mathbf{v}\ , \tag{1}$$

with $(\cdot)^H$ the Hermitian operation. For a general mismatched filter $\mathbf{w}$ of length M ($\geq N$), (1) can alternatively be written as

$$\hat{\mathbf{x}} = \mathbf{W}\mathbf{y} = \mathbf{W}\mathbf{S}\mathbf{x} + \mathbf{W}\mathbf{v} \tag{2}$$

for the LS-MMF convolution matrix $\mathbf{W}$ composed of delay-shifted versions of $\mathbf{w}$ (in the columns).

It is well-known that circular convolution can be performed in the frequency domain via discrete Fourier transform (DFT) of the convolution arguments. Therefore, approximation of $\mathbf{S}$ with the $(L+N-1)\times(L+N-1)$ circulant matrix $\breve{\mathbf{S}}$ by the addition of $(N-1)$ "wrap around" delay shifts of $\mathbf{s}$ [16] yields

$$\begin{aligned}\mathbf{y} &= \mathbf{S}\mathbf{x} + \mathbf{v} \\ &\approx \breve{\mathbf{S}}\overline{\mathbf{x}} + \mathbf{v} \\ &= \mathbf{A}^H((\mathbf{A}\overline{\mathbf{s}}) \odot (\mathbf{A}\overline{\mathbf{x}})) + \mathbf{v},\end{aligned} \tag{3}$$

with $\mathbf{A}$ and $\mathbf{A}^H$ the DFT and inverse DFT (IDFT) matrices, respectively, $\overline{\mathbf{x}}$ and $\overline{\mathbf{s}}$ denoting zero-padding to account for extra vectors in $\breve{\mathbf{S}}$ as well as circular convolution, and $\odot$ the Hadamard product. Consequently, the LS-MMF scattering estimate in (2) becomes

$$\hat{\mathbf{x}} \approx \mathbf{A}^H((\mathbf{A}\overline{\mathbf{y}}) \odot \mathbf{A}\overline{\mathbf{w}}) \tag{4}$$

based on DFTs of the received signal and MMF (denoting as $\overline{\mathbf{y}}$ and $\overline{\mathbf{w}}$ to account for zero-padding). The length of $\hat{\mathbf{x}}$ produced by (4) may not be equal to that produced by (1), due to the various possible filter lengths of $\overline{\mathbf{w}}$. The convolutional tail of $\hat{\mathbf{x}}$ via (4) is a processing artifact and can therefore be ignored.

Fig. 1 illustrates an example of how $\mathbf{S}$ and $\breve{\mathbf{S}}$ are related by depicting a 1 or 0 magnitude in each element (assuming a constant amplitude waveform) for $N = 100$ and $L = 200$. While the approximation in (3) can introduce model mismatch when pulse eclipsing occurs, it is nonetheless commonly used in radar applications, especially those involving wideband operation, to take advantage of the attendant computational savings. Here we examine this efficient filtering approach in the context of

This work was supported in part by Sandia National Laboratories under Contract #2237007 and the Office of Naval Research under Contract #N00014-20-C-1006. This paper describes objective technical results and analysis. Any subjective views or opinions that might be expressed in the paper do not necessarily represent the views of the U.S. Department of Energy or the United States Government. DISTRIBUTION STATEMENT A. Approved for Public Release.

random spectrally-shaped waveforms since the design of $\mathbf{w}$ in this regard likewise employs spectral shaping, and because generation of a new optimized filter for each unique waveform could be computationally prohibitive for some applications.

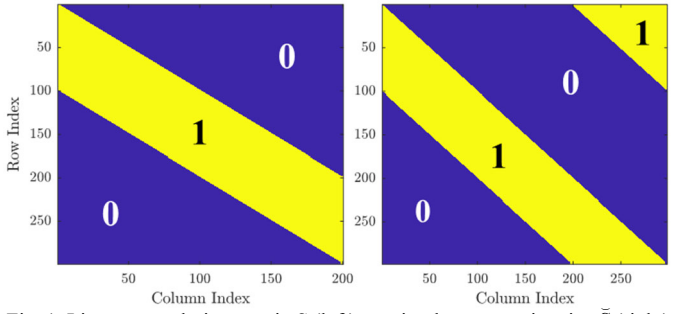

Fig. 1. Linear convolution matrix $\mathbf{S}$ (left) vs. circulant approximation $\breve{\mathbf{S}}$ (right)

III. Least-Squares Mismatched Filtering

The LS-MMF problem was posed in [4] and takes the form

$$\min_{\mathbf{w}} \|\mathbf{g}-\mathbf{S}\mathbf{w}\|_2^2, \tag{5}$$

for $\mathbf{g}$ some desired response (e.g. in [4] an elementary vector). In short, this problem is seeking $\mathbf{w}$ that yields a perfectly whitened response when convolved with discretized waveform $\mathbf{s}$. The regularized closed-form solution to (5) is

$$\mathbf{w}_{\text{LS}} = (\mathbf{S}^H\mathbf{S}+\gamma\mathbf{I})^{-1}\mathbf{S}^H\mathbf{g}, \tag{6}$$

where the scaled identity matrix $\gamma\mathbf{I}$ serves as diagonal loading to ensure full rank (and thus invertibility). This term dominates as positive/real-valued γ increases, in the extreme simplifying to $\mathbf{w}_{\text{LS}} \cong (\gamma\mathbf{I})^{-1}\mathbf{S}^H\mathbf{g} \cong \gamma^{-1}\mathbf{S}^H\mathbf{g}$, a scaled version of the matched filter. Various "beamspoiled" forms of (6) have been examined to provide improved robustness in practical applications [9,11], including zeroing particular rows of $\mathbf{S}$, smoothing across range-straddled versions, and replacing the impulse in elementary vector $\mathbf{g}$ with the nominal matched filter mainlobe. This framework has even been extended to realize a "complementary-on-receive" form across a waveform set [13].

Due to the Fourier relationship between the cross-power spectral density (CPSD) and cross-correlation [17], (5) can equivalently be posed in the frequency domain as

$$\min_{\mathbf{w}} \|\mathbf{A}\mathbf{g}-\mathbf{A}(\mathbf{S}\mathbf{w})\|_2^2, \tag{7}$$

which we shall use to define the relationship to the spectrally-shaped inverse filter. On its face, the solution in (6) has a computational cost that is $O(M^3)$, though exploitation of Toeplitz structure can reduce the cost to $O(M^2)$ [18].

IV. Spectrally-Shaped Inverse Filtering (SIF)

The SIF [18-21] relies on the circulant approximation in (3) and (4), thereby posing a modified version of the LS-MMF problem in (7) as

$$\min_{\mathbf{w}} \|\mathbf{A}\mathbf{g}-\mathbf{A}(\breve{\mathbf{S}}\mathbf{w})\|_2^2. \tag{8}$$

Because the DFT is implicitly assumed to be operating on a single period of a periodic signal [23], this circulant model (conforming to periodicity) facilitates the decomposition

$$\breve{\mathbf{S}} = \mathbf{A}^H\mathbf{D}_{\text{S}}\mathbf{A}, \tag{9}$$

with diagonal matrix $\mathbf{D}_{\text{S}}$ having the DFT of $\overline{\mathbf{s}}$ as its diagonal values. Therefore, the cost function in (8) simplifies to

$$\begin{aligned}\|\mathbf{A}\mathbf{g}-\mathbf{A}(\breve{\mathbf{S}}\mathbf{w})\|_2^2 &= \|\mathbf{A}\mathbf{g}-\mathbf{A}\mathbf{A}^H\mathbf{D}_{\text{S}}\mathbf{A}\mathbf{w}\|_2^2 \\ &= \|\mathbf{g}_{\text{f}}-\mathbf{D}_{\text{S}}\mathbf{w}_{\text{f}}\|_2^2 \\ &= \|\mathbf{g}_{\text{f}}-(\breve{\mathbf{s}}_{\text{f}}\odot\mathbf{w}_{\text{f}})\|_2^2,\end{aligned} \tag{10}$$

where $\mathbf{g}_{\text{f}} = \mathbf{A}\mathbf{g}$ and $\mathbf{w}_{\text{f}} = \mathbf{A}\mathbf{w}$ are DFTs of the (zero-padded) desired response and MMF, respectively, and vector $\breve{\mathbf{s}}_{\text{f}}$ contains the diagonal elements of $\mathbf{D}_{\text{S}}$.

The regularized solution for $\mathbf{w}_{\text{f}}$ in (10) yields the SIF via

$$\begin{aligned}\mathbf{w}_{\text{SIF}} &= (\mathbf{D}_{\text{S}}^H\mathbf{D}_{\text{S}}+\gamma\mathbf{I})^{-1}\mathbf{D}_{\text{S}}^H\mathbf{g}_{\text{f}} \\ &= (\breve{\mathbf{s}}_{\text{f}}^*\odot\mathbf{g}_{\text{f}}) \oslash (|\breve{\mathbf{s}}_{\text{f}}|^2+\gamma) \\ &= \left((\mathbf{A}\breve{\mathbf{s}})^*\odot(\mathbf{A}\mathbf{g})\right) \oslash (|\mathbf{A}\breve{\mathbf{s}}|^2+\gamma),\end{aligned} \tag{11}$$

for Hadamard division $\oslash$ and $|\breve{\mathbf{s}}_{\text{f}}|^2 = \breve{\mathbf{s}}_{\text{f}}\odot\breve{\mathbf{s}}_{\text{f}}^*$. While the first line of (11) is akin to (6), the subsequent steps arise because $\mathbf{D}_{\text{S}}$ is a diagonal matrix, resulting in a computational cost of $O(L\log(L))$ since fast Fourier transforms (FFTs) can be used.

It is important to note that the original convolution matrix $\mathbf{S}$ is not diagonalizable like in (9). Consequently, the efficient SIF approach of (10) and (11) can introduce error, particularly when pulse eclipsing occurs.

V. SIF in the Context of RFM Waveforms

Spectrally-shaped random FM (RFM) waveforms have been demonstrated to expand the operational radar trade-space by greatly increasing signal dimensionality while also being physically amenable to high-power transmitters (see [1] and references therein). The per-pulse sidelobe level that is achievable scales with $10\log_{10}(TB)$, for TB of a single unique waveform. The LS-MMF has been shown [11,24] to provide further sidelobe suppression, being particularly useful to address range sidelobe modulation (RSM) of clutter that can hinder cancellation due to nonstationarity [1,25].

Of course, the LS-MMF can be computationally costly, especially when a completely new filter is required for each waveform. The SIF is therefore a pragmatic solution. Moreover, since both SIF and RFM waveforms rely on spectrum shaping, their relationship bears further consideration.

Let $S_q(f)$ and $W_q(f)$ be the respective waveform spectra and corresponding (matched or mismatched) filter spectra for the qth (of Q) unique RFM waveforms. For desired spectrum shape $|G(f)|$ for both the waveform and filter, ideally we would obtain

$$S_q(f)\times W_q(f) = |G(f)|^2. \tag{12}$$

If waveforms could be designed such that $|S_q(f)| = |G(f)|\ \forall q$, then the matched filter would satisfy (12). However, the time-limited nature of any radar waveform (even CW in practice) requires infinite spectral support, which no practical system can actually accomplish.

The argument can thus be made that mismatched filtering is better suited to more closely approximate (12) because doing so permits more degrees of freedom. Indeed, rearrange (12) as

$$W_q(f) = \frac{|G(f)|^2}{S_q(f)} \tag{13}$$

and the form of a spectrally-shaped inverse filter (SIF) emerges. However, the presence of $S_q(f)$ in the denominator implies the existence of poles not at the origin (in the z-transform domain), which is to say that (13) is an infinite impulse response (IIR) filter (as observed in [25]). Noting again that radar operation occurs on time-limited intervals (e.g. the receive interval between pulses) consequently means that truncation of the ideal $W_q(f)$ is necessary in practice, which translates into error.

For instance, Fig. 2 illustrates the magnitude envelope of the SIF obtained via (11) for different amounts of zero-padding, thereby controlling the degree of truncation. The waveform is a super-Gaussian shaped RFM with shaping parameter $n = 8$ [26,27] and discretized length $N = 100$. The matched filter magnitude is also plotted for comparison. The factor C indicates the multiplicative increase in MMF length via zero-padding, so that $M = CN$. We clearly see that increasing filter length exhibits an extended tail that is being truncated, with an attendant reduction in error (though never completely avoided).

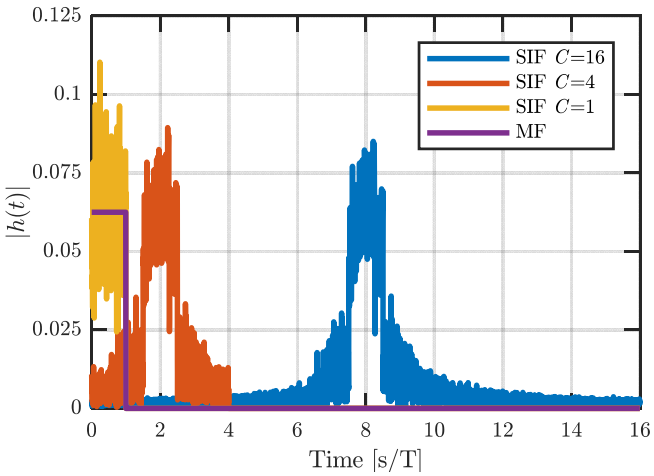

Fig 2: Impulse response comparison of shaped inverse filters based on degree of zero-padding of $\mathbf{s}$ and $\mathbf{g}$ to form filter $\mathbf{w}_{\text{SIF}}$ of length $M = CN$

VI. Shaping Selection & Assessment Metrics

One could argue that the Gaussian power spectral template is ideal because the associated Fourier counterpart is likewise a Gaussian autocorrelation that theoretically has no sidelobes. Of course, the roll-off of the Gaussian power spectrum also requires a not insignificant degree of "over-sampling" (relative to 3-dB bandwidth) that incurs both memory and computational costs and could be outright infeasible for wideband operation.

Consequently, in [26,27] the super-Gaussian structure from optics was considered for RFM waveform design and then experimentally demonstrated. In short, shape parameter n can be set as low as 2 (standard Gaussian), with $n \to \infty$ approaching a rectangular shape that is completely bandlimited (with attendant sinc(·) matched filter sidelobe response). Within these extremes is a trade-off between improving spectral containment and larger close-in "persistent" sidelobes as n increases (i.e. not reduced by incoherent sidelobe averaging via slow-time processing). We shall examine selected values of n to illustrate general behavior, though a larger catalogue of spectral templates can also be found in [28].

Using $\mathbf{s}^{(k)}$ to denote the kth optimization iteration of the discretized form of waveform $s(t)$, the total mean-squared deviation (MSD) can be written as

$$\Delta_k = \mathbf{1}^T \left(\left| \left[(\mathbf{A}\mathbf{s}^{(k)}) \odot (\mathbf{A}\mathbf{s}^{(k)})^* \right] - \left[\mathbf{g}_{\text{f}} \odot \mathbf{g}_{\text{f}}^* \right] \right|^2 \right), \tag{14}$$

with $\mathbf{g}_{\text{f}}$ the discretization of $G(f)$ and $\mathbf{1}$ a vector of ones. The MSD is useful to assess convergence for waveform design methods based on template matching.

Another useful metric is mismatch loss (MML)

$$\Gamma_k = \frac{\left\| \mathbf{s}^{(k)} \right\|_2^2 \left\| \mathbf{w}^{(k)} \right\|_2^2}{\max \left\{ \left| s^{(k)}[n] * w^{(k)}[n] \right|^2 \right\}}, \tag{15}$$

which determines the signal-to-noise ratio (SNR) loss of a given MMF compared to the matched filter. Here $\mathbf{w}^{(k)}$ is the MMF computed from the kth iteration of waveform $\mathbf{s}^{(k)}$, with $w^{(k)}[n]$ and $s^{(k)}[n]$ the nth sample of each. This loss is incurred as a by-product of suppressing sidelobes. Moreover, with (12) satisfied by the matched filter under the ideal condition $|S_q(f)| = |G(f)|$, we can infer that mismatch loss in (15) should decrease as waveform optimization iteratively approaches the desired spectrum shape (i.e. as (14) decreases).

Finally, in addition to the fixed template $G(f)$ for both waveform and MMF generation, an alternative specifically for MMF design arises from minimizing an analytical form of MSD, yielding the ensemble average from waveform design via

$$\bar{G}(f) = \sqrt{\frac{1}{Q} \sum_{q=1}^{Q} |S_q(f)|^2}. \tag{16}$$

Consequently, the discretized form $\mathbf{g}_{\text{f}}$ in the SIF formulation of (11) could be replaced with

$$\bar{\mathbf{g}}_{\text{f}}^{(k)} = \left(\frac{1}{Q} \sum_{q=1}^{Q} \left[(\mathbf{A}\mathbf{s}^{(k)}) \odot (\mathbf{A}\mathbf{s}^{(k)})^* \right] \right)^{0.5}, \tag{17}$$

noting the square-root is computed on a per-element basis.

VII. MMF for Random FM (Simulation Results)

As an example, Fig. 3 illustrates how MML from (15) is affected by the convergence of a spectrally-shaped RFM method. Specifically, $Q = 100$ pseudo-random optimized (PRO-FM) waveforms were generated according to [27] for 10^4 iterations, using (super-Gaussian) $n = 2$, 8, and 32, and over-sampled by a factor of 4 relative to 3-dB bandwidth (to capture spectral roll-off). At each iteration, (14) and (15) were computed and averaged across all 100 waveforms (having independent, random initializations). In Fig. 4 we see that MML from (15) and MSD from (14) are clearly related, with a nearly linear relationship in how each metric decreases as optimization progresses. In other words, better waveform template matching translates to lower loss in the associated SIF mismatched filter.

Now using (super-Gaussian) $n = 4$, $TB = 64$, and again over-sampling 3-dB bandwidth by 4, we compare the different filter responses. Specifically, the matched filter, the LS-MMF from (6), and SIF from (11) are examined. The SIF uses either the original ideal template $G(f)$ – denoted "Template SIF" – or the

average waveform spectrum response via (17), denoted "Average SIF". While the matched filter clearly has the same length N as the waveform, the MMF cases are set to have length $3N$. Finally, since doing so has been shown to work well [11], the LS-MMF desired response $\mathbf{g}$ is set to all zeroes except for the matched filter mainlobe, which in this case is taken from the inverse DFT of the $n = 4$ super-Gaussian spectral template.

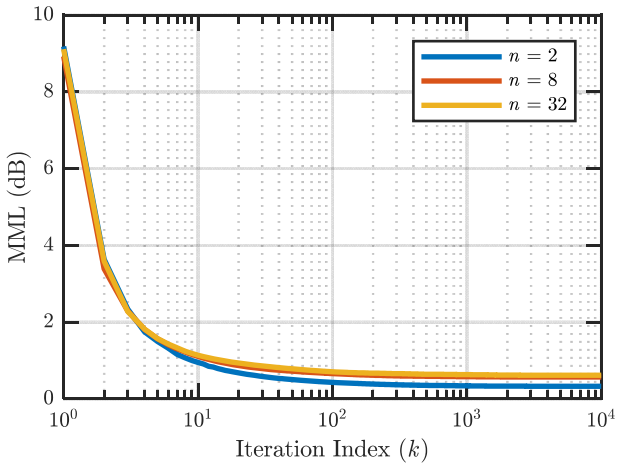

Fig 3: Mismatch loss (MML) of SIF vs. iteration for different super-Gaussian parameters and averaged across 100 independent PRO-FM waveforms

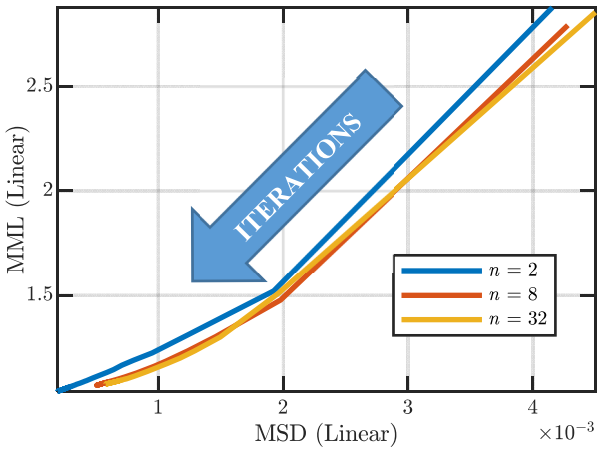

Fig 4: Mismatch loss (MML) of SIF vs. MSD for different super-Gaussian parameters and averaged across 100 independent PRO-FM waveforms

Consider a single PRO-FM waveform optimized for 1000 iterations, ensuring MML convergence (per Fig. 3). Then Fig. 5 illustrates the ensuing different filter responses, where the matched filter (as expected) yields the highest sidelobes but no mismatch loss. We see that LS-MMF largely compensates for the "persistent" sidelobe roll-off arising from the super-Gaussian template [26,27], though it also incurs a 1.80 dB mismatch loss. The Average SIF further suppresses sidelobes (away from the mainlobe) while reducing MML to 0.99 dB. However, the real winner is Template SIF, which exhibits no meaningful sidelobe floor and a MML of 1.03 dB.

Doing likewise for each of the $Q = 100$ unique waveforms and then performing slow-time processing for zero Doppler (i.e. a coherent sum) realizes the filter responses in Fig. 6. Since the waveforms are unique, we expect to observe $10 \log_{10}(100) = 20$ dB of further sidelobe suppression due to incoherent averaging (mainlobes still combine coherently). The exception to this sidelobe trend is the Average SIF case, which is essentially unchanged between the single-waveform (Fig. 5) and coherent combining (Fig. 6) results, suggesting that the benefit of combining already occurred via (17). Put another way, the filtered data already matches the desired response and thus no additional reduction in variance occurs.

The LS-MMF mismatch loss is now 1.78 dB, nearly unchanged from the single-waveform case. However, the Average SIF and Template SIF losses now shift some to 0.91 and 1.09 dB, respectively. The relatively low loss and lack of a sidelobe floor for the Template SIF make it an attractive choice.

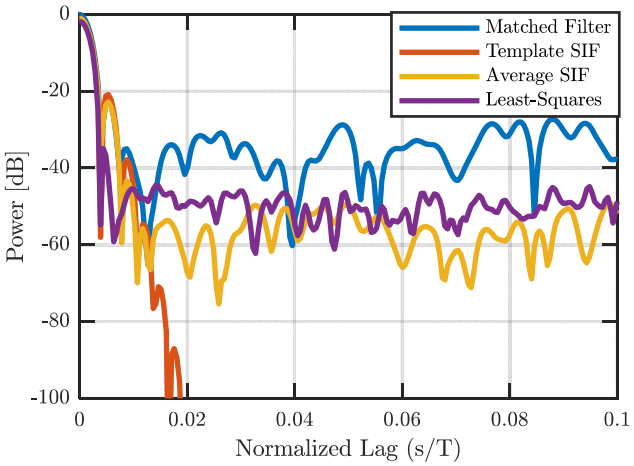

Fig 5: Filter response comparison for single PRO-FM waveform designed according to $n = 4$ super-Gaussian spectral template

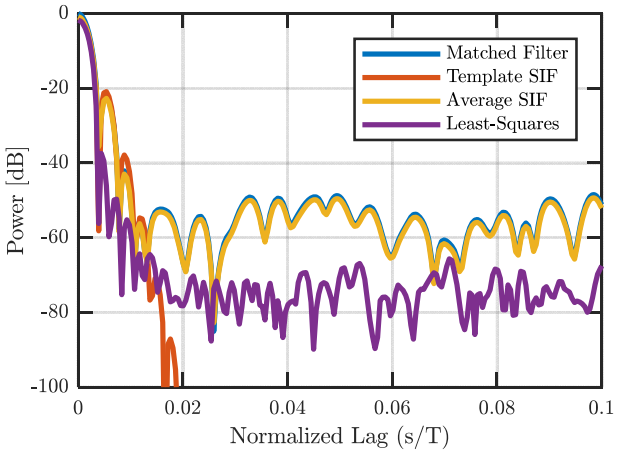

Fig 6: Filter response comparison after coherent slow-time combining of 100 PRO-FM waveforms designed according to $n = 4$ super-Gaussian template

VIII. MMF FOR RANDOM FM (EXPERIMENTAL RESULTS)

To experimentally assess the various waveform/filter combinations, a set of 5000 unique PRO-FM waveforms [11] were designed and physically transmitted to produce a 200 ms CPI. Another 200 ms CPI of 5000 repeated pulses (using a single PRO-FM waveform) was also generated for comparison. Each pulse had a 1.28 μs pulsewidth and a 3-dB bandwidth of 50 MHz, yielding a per-pulse $TB = 64$ at a center frequency of 3.45 GHz. Open-air measurements were processed using the matched filter and Template SIF.

Open-air results for the pulse-repeated CPI are shown in Fig 7, with the matched filter in the top panel and Template SIF in the bottom. While several movers are visible in both cases, the former reveals sidelobe roll-off (in range) as vertical streaks associated with some of the larger mover responses. These artifacts are clearly suppressed in the SIF case. Note that the noise + interference floor for both is virtually identical since the use of a single repeated waveform avoids range sidelobe modulation (RSM).

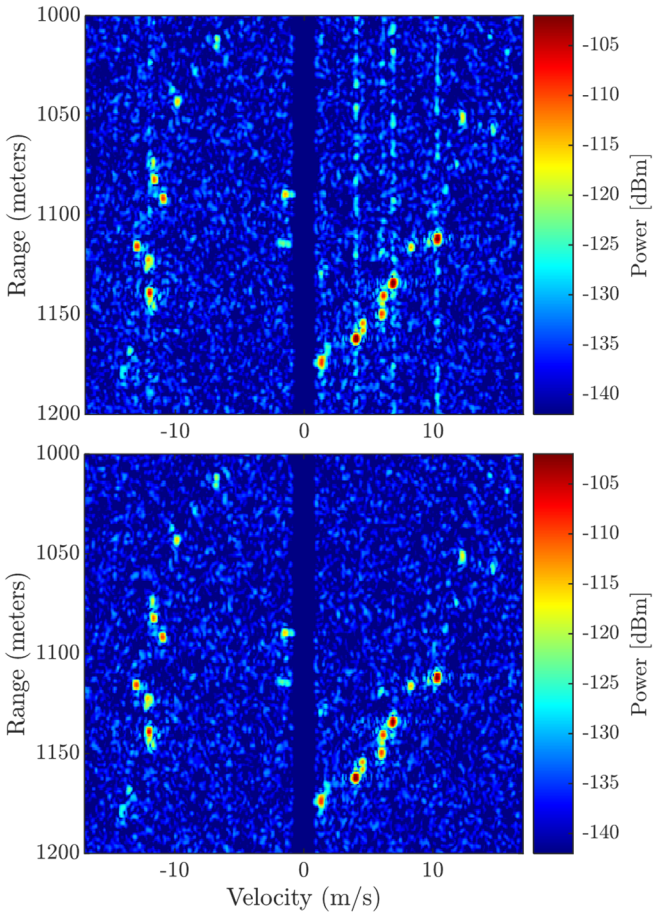

Fig 7: Open-air range/Doppler responses for a single repeated PRO-FM waveform after simple projection-based clutter cancellation using the matched filter (top) and Template SIF (bottom)

The processing in Fig. 7 was then duplicated for the open-air measurements shown in Fig. 8 where each waveform is unique, such that incoherent sidelobe averaging occurs (and associated RSM). These data collections occurred back-to-back, so while not identical they are qualitatively the same.

Visual inspection of the matched filter (top) and SIF (bottom) responses in Fig. 8 reveals no discernible difference. However, the cause for such similarity is the modest dynamic range achievable for this data collection given that incoherent sidelobe averaging has already pushed down sidelobes by an additional $10\log_{10}(5000) = 37$ dB. Numerical assessment shows the SIF result does exhibit a 1.1 dB lowering in the noise + interference floor, which could clearly be much greater in a high dynamic range scenario.

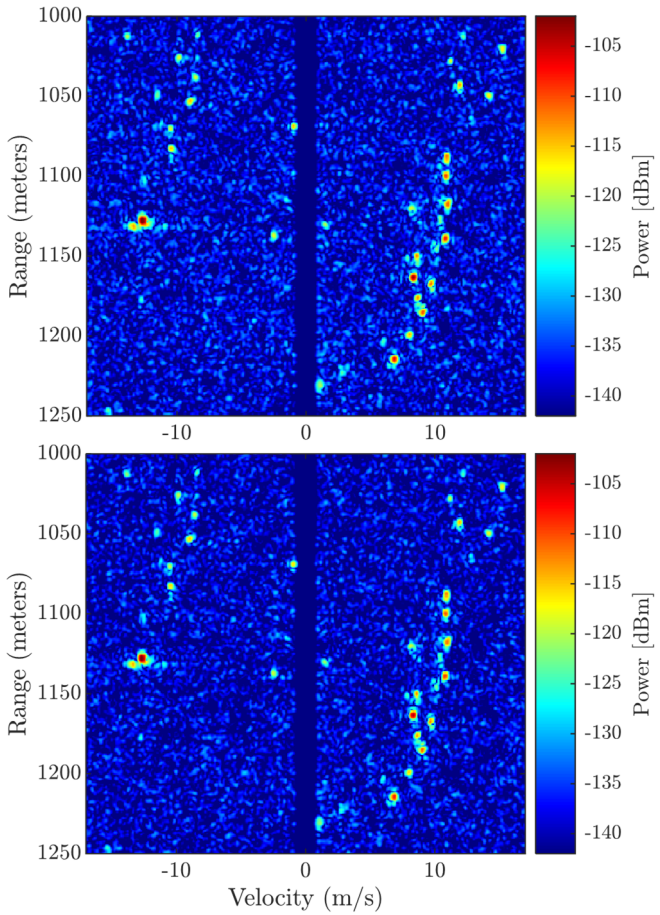

Fig 8: Open-air range/Doppler responses for unique PRO-FM waveforms after simple projection-based clutter cancellation using the matched filter (top) and Template SIF (bottom)

Finally, in the interest of completeness, the degradation that the SIF can incur when model mismatch arises is worth examining. To emulate this effect, the beginning of each PRI for the nonrepeating waveform case from Fig. 8 was range-gated by half of the pulsewidth. This seemingly arbitrary amount serves to eclipse the direct-path between the separate transmit and receive antennas used in the data capture, thereby invalidating the approximation used in the circulant model. Fig. 9 illustrates the result, again for the matched filter and SIF, where the former is no different from Fig. 8 since the observed traffic intersection is far enough away, but the latter experiences nearly 10 dB of degradation in the form of sidelobe increase. Consequently, we see that proper selection of the range interval for which SIF is applied is clearly important as a means to mitigate this effect.

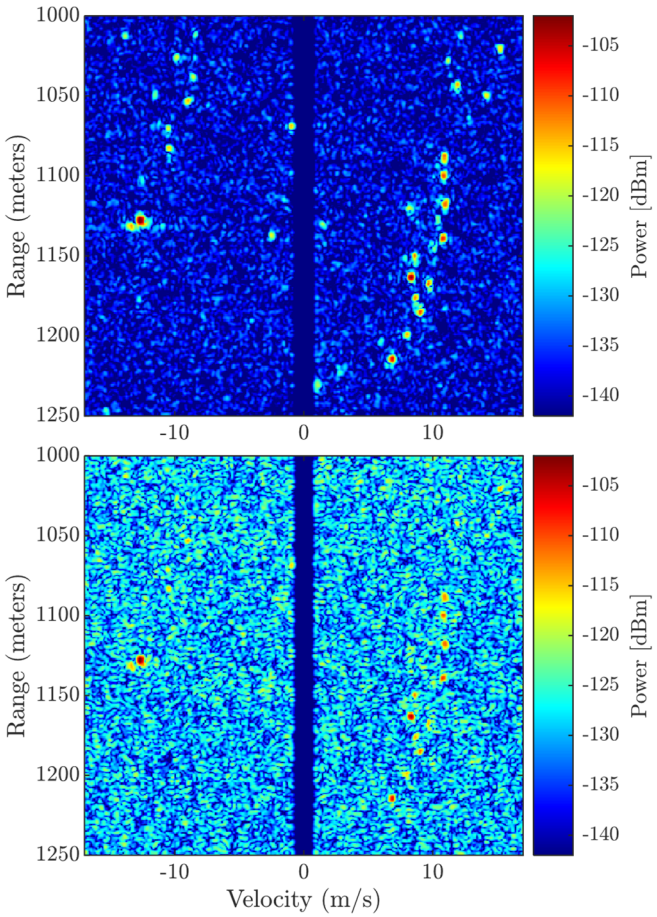

Fig 9: Pulse-eclipsed open-air range/Doppler responses for unique PRO-FM waveforms after simple projection-based clutter cancellation using the matched filter (top) and Template SIF (bottom)

IX. Conclusions

The spectrally-shaped inverse filter (SIF) is attractive as a way to obtained optimized mismatched filters (MMF) that can be implemented in a computationally efficient manner, especially when unique waveforms dictate generation of new MMFs. Moreover, with many random FM (RFM) waveforms likewise being designed via spectrum shaping, there is a natural connection between the two whereby the goodness of fit to the design template is directly related to the MMF mismatch loss. Experimental results demonstrate the efficacy of this waveform/filter combination, with the cautionary note that eclipsing can impose significant degradation.

REFERENCES

[1] S.D. Blunt, *et al*, "Principles & applications of random FM radar waveform design," *IEEE Aerospace & Electronic Systems Mag*., vol. 35, no. 10, pp. 20-28, Oct. 2020.

[2] P.M. McCormick, S.D. Blunt, "Nonlinear conjugate gradient optimization of polyphase-coded FM radar waveforms," *IEEE Radar Conf*., Seattle, WA, May 2017.

[3] C.A. Mohr, P.M. McCormick, C.A. Topliff, S.D. Blunt, J.M. Baden, "Gradient-based optimization of PCFM radar waveforms," *IEEE Trans. Aerospace & Electronic Systems*, vol. 57, no. 2, pp. 935-956, Apr. 2021.

[4] M.H. Ackroyd, F. Ghani, "Optimum mismatched filters for sidelobe suppression," *IEEE Trans. Aerospace & Electronic Systems*, vol. AES-9, no. 2, pp. 214-218, March 1973.

[5] K.R. Griep, J.A. Ritcey, J.J. Burlingame, "Poly-phase codes and optimal filters for multiple user ranging," *IEEE Trans. Aerospace & Electronic Systems*, vol. 31, no. 2, pp. 752-767, Apr. 1995.

[6] J.E. Cilliers, J.C. Smit, "Pulse compression sidelobe reduction by minimization of Lp-norms," *IEEE Trans. Aerospace & Electronic Systems*, vol. 43, no. 3, pp. 1238-1247, July 2007.

[7] A. De Maio, Y. Huang, M. Piezzo, S. Zhang, and A. Farina, "Design of radar receive filters optimized according to Lp-norm based criteria," *IEEE Trans. Signal Processing*, vol. 59, no. 8, pp. 4023-4029, May 2011.

[8] U.C. Doyuran, R.F. Tigrek, "M-ary CPM pulse compression filter design for low, flat sidelobes," *Intl. Radar Conf*., Lille, France, Oct. 2014.

[9] D. Henke, P. McCormick, S.D. Blunt, T. Higgins, "Practical aspects of optimal mismatch filtering and adaptive pulse compression for FM waveforms," *IEEE Intl. Radar Conf*., Washington, DC, May 2015.

[10] O. Rabaste, L. Savy, "Mismatched filter optimization for radar applications using quadratically constrained quadratic programs," *IEEE Trans. Aerospace & Electronic Systems*, vol. 51, no. 4, pp. 3107-3122, Oct. 2015.

[11] J. Jakabosky, S.D. Blunt, B. Himed, "Spectral-shape optimized FM noise radar for pulse agility," *IEEE Radar Conf*., Philadelphia, PA, May 2016.

[12] S.D. Blunt, E.L. Mokole, "An overview of radar waveform diversity," *IEEE Aerospace & Electronic Systems Mag.*, vol. 31, no. 11, pp. 2-42, Nov. 2016.

[13] C.C. Jones, C.A. Mohr, P.M. McCormick, S.D. Blunt, "Complementary frequency modulated radar waveforms and optimised receive processing," *IET Radar, Sonar & Navigation*, vol. 15, no. 7, pp. 708-723, Apr. 2021.

[14] M. Coutino, F. Uysal, L. Anitori, "Waveform-aware optimal window function design for mismatched filtering," *IEEE Radar Conf*., New York City, NY, Mar. 2022.

[15] U. Pe'er, N. Yang, "Choosing the optimal parameters for mismatched filter design," *IEEE Radar Conf*., New York City, NY, Mar. 2022.

[16] R.M. Gray, "Toeplitz and Circulant Matrices: A Review," *Foundations and Trends in Communications and Information Theory*, vol. 2, no. 3, pp 155-239, Jan. 2006.

[17] K. Shanmugan, A.M. Breipohl, *Random Signals: Detection Estimation and Data Analysis*, John Wiley & Sons, 1988.

[18] M.H. Hayes, *Statistical Digital Signal Processing and Modeling*, 1st Ed. John Wiley & Sons, 1996

[19] S. Senmoto, D.G. Childers, "Signal resolution via digital inverse filtering," *IEEE Trans. Aerospace and Electronic Systems*, vol. AES-8, no. 5, pp. 633-640, Sept. 1972.

[20] R.C. Daniels, V. Gregers-Hansen, "Code inverse filtering for complete sidelobe removal in binary phase coded pulse compression systems," *IEEE Intl. Radar Conf*., Arlington, VA, May 2005.

[21] J. Moll, V. Krozer, "Time-varying inverse filtering of range-compressed radar signals," *German Microwave Conf.,* Ilmenau, Germany, Mar. 2012.

[22] R. Zemmari, B. Knoedler, U. Nickel, "GSM passive coherent location: Improving range resolution by mismatched filtering," *IEEE Radar Conf.*, Ottawa, Canada, Apr. 2013.

[23] J.G. Proakis, D.K. Manolakis, *Digital Signal Processing – Principles, Algorithms, & Applications*, 3rd ed., Prentice-Hall, 1995.

[24] B. Ravenscroft, J.W. Owen, S.D. Blunt, A.F. Martone, K.D. Sherbondy, "Optimal mismatched filtering to address clutter spread from intra-CPI variation of spectral notches," *IEEE Radar Conf*., Boston, MA, Apr. 2019.

[25] S.D. Blunt, M.R. Cook, J. Stiles, "Embedding information into radar emissions via waveform implementation," *Intl. Waveform Diversity & Design Conf*., Niagara Falls, Canada, Aug. 2010.

[26] C.A. Mohr, S.D. Blunt, "Designing random FM radar waveforms with compact spectrum," IEEE Intl. Conf. Acoustics, Speech & Signal Processing, Toronto, Canada, June 2021.

[27] M.B. Heintzelman, T.J. Kramer, S.D. Blunt, "Experimental evaluation of super-Gaussian-shaped random FM waveforms," *IEEE Radar Conf.*, New York City, NY, Mar. 2022.

[28] A.W. Doerry, "Catalog of window taper functions for sidelobe control," Sandia Technical Report, SAND2017-4042, Apr. 2017.